

# Conservative Global Gyrokinetic Toroidal Full- $f$ 5D Vlasov Simulation

Y. Idomura<sup>1,2</sup>, S. Tokuda<sup>2,1</sup>, N. Aiba<sup>2</sup>, and H. Urano<sup>2</sup>

<sup>1</sup>Japan Atomic Energy Agency, Higashi-Ueno 6-9-3, Taitou, Tokyo, 110-0015, Japan

<sup>2</sup>Japan Atomic Energy Agency, Mukouyama 801-1, Naka, Ibaraki, 311-0193, Japan

E-mail address of main author: [idomura.yasuhiro@jaea.go.jp](mailto:idomura.yasuhiro@jaea.go.jp)

**Abstract:** A new global gyrokinetic toroidal full- $f$  five dimensional (5D) Vlasov simulation (GT5D) [1] is developed using a novel non-dissipative conservative finite difference scheme (NDCFD) [2], which guarantees numerical stability by satisfying relevant conservation properties of the modern gyrokinetic theory. By using GT5D, robust and accurate long time simulations of tokamak micro-turbulence are enabled for the first time based on a full- $f$  approach with self-consistent evolutions of equilibrium profiles balanced with sources. GT5D is verified through comparisons of zonal flow damping tests, and linear and nonlinear analyses of ion temperature gradient driven (ITG) modes against a global gyrokinetic toroidal  $\mathcal{J}$  particle-in-cell (PIC) simulation (GT3D) [3]. The neoclassical physics is implemented using the linear Fokker-Planck (FP) collision operator, and the equilibrium radial electric field  $E_r$  is determined self-consistently. In a normal shear tokamak, source driven ITG turbulence simulations are performed using sources which fix power input near the axis and the ion temperature  $T_i$  at the edge, respectively, and profile evolutions are traced over a collision time. It is found that a significant part of the heat flux is carried by avalanches in source free regions, where stiff  $T_i$  profiles are sustained with globally constant  $L_{ii}$  at slightly above the critical value. In this region, the equilibrium  $E_r$  becomes significantly larger than the neoclassical level, and its shear strongly affects the directions of the avalanche propagation and the momentum flux. A non-diffusive momentum flux due to the  $E_r$  shear is observed and non-zero (intrinsic) toroidal rotation is sustained without momentum input near the axis.

## 1. Introduction

5D gyrokinetic simulations are essential tools to study anomalous turbulent transport in tokamak plasmas. Although a number of gyrokinetic simulations have been developed so far, most of existing simulations are  $\mathcal{J}$  simulations in an isolated system without sources and collisions or in an open system with fixed gradients. The fixed gradient approach has been successful in estimating steady transport levels for profiles given based on the experiment, but it still has difficulty in addressing open issues such as the profile stiffness, transient transport properties, and the formation of transport barriers. In particular, it is very difficult to simulate turbulent transport with stiff profiles, because the experimental data contain a finite error and a slight change in gradients leads to a large increase in the turbulent flux. In order to address such open issues, we need a new gyrokinetic simulation based on a full- $f$  approach, in which equilibrium profiles and turbulent fluctuations are evolved self-consistently following the first principles. In this work, we develop a new global gyrokinetic toroidal full- $f$  5D Vlasov simulation GT5D [1] using the NDCFD [2], which satisfies high numerical accuracy and stability required in a full- $f$  approach. In addition to experimentally relevant source models, the linear FP collision operator is implemented to keep the neoclassical physics which is essential in dictating the equilibrium  $E_r$ . After showing the verification of GT5D through linear and nonlinear benchmarks against GT3D and neoclassical benchmarks, source driven ITG turbulence simulations are presented. In the simulation, long time evolutions of the turbulent transport and profile formations are solved self-consistently in open system tokamak plasmas with sources and collisions, and the ion heat and momentum transport and stiff  $T_i$  profiles in a normal shear tokamak is addressed.

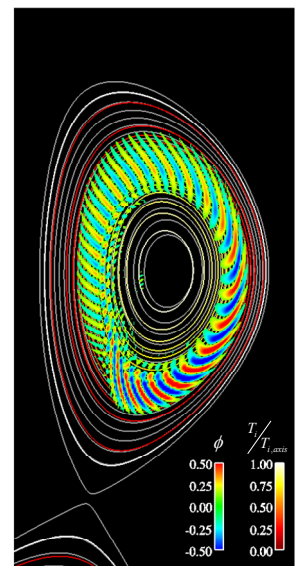


Fig. 1: The ITG mode in JT60SA with ITER-like configuration.

## 2. Conservative global Gyrokinetic Toroidal full- $f$ 5D Vlasov code GT5D

In the present study, we consider the electrostatic ITG turbulence described by gyrokinetic ions and adiabatic electrons in a tokamak configuration. In the modern gyrokinetic theory [4], the gyrokinetic equations are given using the gyro-centre Hamiltonian  $H=m_i v_{||}^2/2+\mu B+e\langle\phi\rangle_\alpha$  and the Poisson bracket (PB) operator  $\{, \}$  in the gyro-centre coordinates  $\mathbf{Z}=(t, \mathbf{R}, v_{||}, \mu, \alpha)$ ,

$$\begin{aligned} \frac{\partial f}{\partial t} + \{f, H\} &= C(f) + S, \\ -\nabla_\perp \cdot \frac{\rho_{ii}^2}{\lambda_{Di}^2} \nabla_\perp \phi + \frac{1}{\lambda_{De}^2} (\phi - \langle\phi\rangle_f) &= 4\pi e \left[ \int f \delta([\mathbf{R} + \boldsymbol{\rho}] - \mathbf{x}) d^6 Z - n_{0e} \right], \end{aligned} \quad (1)$$

where  $\mathbf{R}$  is a guiding centre position,  $\mathbf{R} + \boldsymbol{\rho}$  is a particle position,  $v_{||}$  is the parallel velocity,  $\mu$  is the magnetic moment,  $\alpha$  is the gyro-phase angle,  $f$  is the guiding centre distribution function,  $n_{0e}$  is the equilibrium electron density,  $\rho_{ii}$  is the ion Larmor radius,  $\lambda_{De}$ ,  $\lambda_{Di}$  are the Debye lengths,  $\phi$  is the electrostatic potential,  $\langle \rangle_\alpha$ ,  $\langle \rangle_f$  are the gyro-phase and flux-surface average operators, respectively, and  $C$  and  $S$  are collision and source terms described below. In full- $f$  simulations, it is extremely important to treat the PB operator using a numerical scheme which satisfies relevant conservation properties, because full- $f$  nonlinear simulations easily blow up without such physical constraints. The NDCFD suppresses numerical instabilities by conserving the phase space volume and two invariants,  $f$  and  $f^2$ , which are inherent to the PB operator. GT5D uses the 4th order NDCFD, which enables robust and accurate long time full- $f$  simulations beyond turbulent time scales. The other techniques used in GT5D are implicit time integration for stiff linear terms based on the 2nd order additive semi-implicit Runge-Kutta method [5], a finite element gyrokinetic Poisson solver with a full finite Larmor radius (FLR) operator [1], a full radius treatment of shaped magnetic equilibria including the magnetic axis, and interfaces to the database of the JT60U experiment and the JT60SA design (Fig.1). The collision term  $C$  is essential for long time gyrokinetic simulations, in which fine scale velocity space structures produced by the phase mixing due to parallel streaming have to be smeared out by physical dissipation. In addition, the collisional effect itself is important in gyrokinetic simulations. The neoclassical physics determines relevant kinetic equilibrium with  $E_r$ , which plays key roles in various turbulent phenomena. The neoclassical transport becomes dominant when the turbulence is suppressed. To keep the standard neoclassical physics in core plasmas, we solve the linear FP collision operator [6],

$$C(f) = \frac{\partial}{\partial s} (v_{s\perp} v^2 f) + \frac{\partial}{\partial u} (v_{s||} u f) + \frac{1}{2} \frac{\partial^2}{\partial s^2} (v_\perp v^4 f) + \frac{1}{2} \frac{\partial^2}{\partial u^2} (v_{||} v^2 f) + \frac{\partial^2}{\partial s \partial u} (v_{||\perp} v^3 f) + C_F, \quad (2)$$

where  $s=2\mu B/m_i$ ,  $u=v_{||}-U_{||}$  are the moving frame with respect to the parallel flow velocity  $U_{||}$ ,  $v^2=u^2+s$ , and  $C_F$  involves a field particle operator [7] and a correction term which keeps exact conservations of the particle, the momentum, and the energy. In GT5D, Eq.(2) is solved using the 6th order centred finite difference, and the moving frame and coefficients  $v_{s\perp}$ ,  $v_{s||}$ ,  $v_\perp$ ,  $v_{||}$ ,  $v_{||\perp}$  [6] are determined using time dependent equilibrium profiles, which provide indirect nonlinear effects on  $C$ . The source term  $S$  requires some empirical modelling. Near the axis, we use a model to fix power input,  $S_{src}=A_{src}(\mathbf{R})(f_{M1}-f_{M2})$ , where a deposition profile  $A_{src}$  and Maxwellian distributions  $f_{M1}$ ,  $f_{M2}$  are given to fix  $P_{in}=\int (m_i v^2/2) S_{src} d^6 Z$  (and  $\int S_{src} d^6 Z=0$ ,  $\int v_{||} S_{src} d^6 Z=0$ ). On the other hand, in the edge,  $T_i$  (and  $U_{||}$ ) is fixed by a Krook type operator,  $S_{snk}=\tau_s^{-1} A_{snk}(\mathbf{R})(f_0-f)$ , reflecting a boundary region of H-mode plasmas where  $T_i$  is limited by edge localized modes and  $U_{||}\sim 0$  because of charge exchange with the neutrals tied to the wall.

### 3. Numerical verification of GT5D

Since GT5D involves both neoclassical and turbulent transport phenomena, we test these qualitatively different physics independently. The turbulent transport, which is essentially nonlinear, is checked through benchmarks against GT3D in the collisionless limit. On the other hand, the neoclassical transport is tested against standard local theories.

**Linear benchmark** In the benchmark, we use a circular concentric tokamak configuration with  $R_0/a=2.8$ ,  $a/\rho_{ti}=150$ , and  $q(r)=0.85+2.18(r/a)^2$ . In the linear ITG benchmark ( $R_0/L_n=2.22$ ,  $R_0/L_{ti}=6.92$ ), both the eigenfrequency spectra (Fig.2(a)) and the eigenfunctions show excellent agreements. In the zonal flow damping tests ( $L_n=L_{ti}=\infty$ ), zonal flow amplitudes in Fig.2(b) coincide with each other, and both results agree with a theoretical prediction [8] in the real frequency, the damping rate, and the residual flow level. In Fig.3(c), the perturbed distribution function  $\delta f$  clearly shows coherent (filament) structures of trapped (passing) particles due to the neoclassical polarization (the ballistic mode), which dictates residual flow levels.

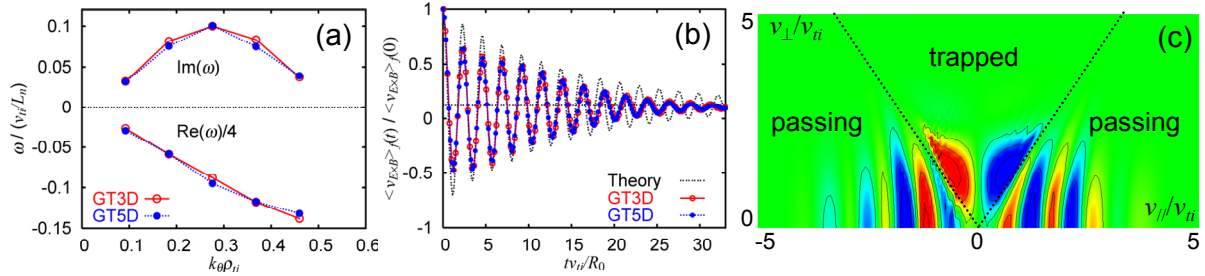


Fig.2: (a) Eigenfrequency spectra of the ITG mode. (b) flux-surface averaged zonal flows observed in zonal flow damping tests using GT3D and GT5D. (c) velocity space structures of  $\delta f = f - f_0$  ( $r=0.5a$ ,  $\theta=0$ ) are resolved using  $128 \times 32$  velocity grids in GT5D.  $v_{\parallel}$  grids are aligned to filament structures of the ballistic mode.

**Nonlinear ITG benchmark** Figure 3 shows ITG turbulence simulations ( $R_0/L_n=2.22$ ,  $R_0/L_{ti}=6.92$ ) without sources and collisions. In sourceless simulations, the turbulent transport is quenched in the final stage, and the system is relaxed to nonlinear marginal states given by the Dimits shift [9]. In Fig.3(a), both results give the same initial saturation amplitudes, and then,  $T_i$  profiles are relaxed to the nonlinear critical gradient at  $R/L_{ti} \sim 5.8$ , which is far above the linear critical gradient  $R/L_{ti} \sim 4.5$ . Spatio-temporal evolutions of zonal flows in Figs.3(b) and (c) show similar initial bursts followed by spreading of turbulent regions with almost the same propagation velocities, and the final stage is dominated by global quasi-steady zonal flows. In the quasi-steady phase, turbulent correlation lengths show quantitative agreements with  $\Delta r \sim 6\rho_{ti}$  [1]. From these results, collisionless turbulent dynamics in GT5D is verified.

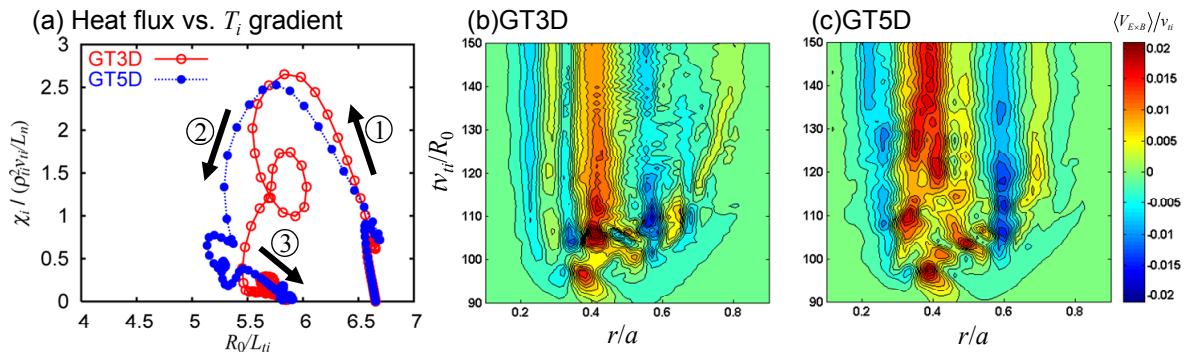


Fig.3: Nonlinear ITG turbulence simulations using GT3D ( $\sim 2000$  particles/cell) and GT5D ( $(N_R, N_{\zeta}, N_Z, N_{v_{\parallel}}, N_{v_{\perp}}) = (160, 32, 160, 128, 32)$ ).  $1/3$  wedge torus model is used. (a) shows evolutions of the ion heat diffusivity  $\chi_i$  vs.  $L_{ti}$ . (b) and (c) show spatio-temporal evolutions of flux-surface averaged zonal flows.

**Neoclassical benchmark** Although GT5D can simulate steep profiles and low aspect ratio configurations with finite orbit width effects, in the benchmark, we use a relatively large aspect ratio configuration ( $R_0/a=5$ ) with moderate gradients ( $R_0/L_n=1$ ,  $R_0/L_{ti}=1$ ) to make quantitative comparisons with standard local theories. The other parameters are the same as ITG benchmarks, and the collisionality is  $\nu^* \sim 0.1$ . We perform axisymmetric simulations starting from a local Maxwellian distribution  $f_{LM}$ . Since the PB operator does not annihilate  $f_{LM}$ ,  $E_r$  quickly develops in a transit time and the geodesic acoustic mode (GAM) is excited. Through the damping of GAMs, initial quasi-steady  $E_r$  develops to satisfy the ambipolar condition (zero particle flux with adiabatic electrons, Fig.4 (a)), and then, the system gradually approaches to the neoclassical solution. It is noted that in the above collisionless ITG simulations, a gyrokinetic Vlasov equilibrium  $f_{CM}$  defined by  $\{f_{CM}, H_0\}=0$  is used, and the equilibrium  $E_r$  is not taken into account. In the benchmark, we recover standard local theories except for the following new findings: 1) During GAM oscillations, significant heat flux is produced by coupling between up-down asymmetric GAM perturbations and the magnetic drift (Fig. 4(a)). 2) the ion heat flux agrees with Chang-Hinton's formula [10] when we keep only  $m=0$ ,  $n=0$  component of  $\phi$ , but additional heat flux is produced with  $m \neq 0$ ,  $n=0$  component of  $\phi$  (Fig.4 (b)), where  $m$ ,  $n$  are poloidal and toroidal mode numbers, respectively. 3) the equilibrium  $E_r$  agrees with the standard force balance relation [11] (Fig.4 (c)),

$$\langle U_{||} \rangle_f = \frac{T_i I}{m_i \Omega_i} \left( \frac{d\psi}{dr} \right)^{-1} \left[ (k-1) \frac{d \ln T_i}{dr} - \frac{d \ln n_i}{dr} + \frac{e}{T_i} E_r \right], \quad (3)$$

where  $\psi$  is the poloidal flux,  $\Omega_i$  is the ion gyro-frequency, and  $k$  is determined by the neoclassical theory. However,  $E_r$  approaches to Eq.(3) slowly in collisional time scales starting from initial  $E_r$  close to a condition  $k \sim 0$ . As a result, initial  $E_r$  is significantly larger than the neoclassical level, when temperature gradient is finite.

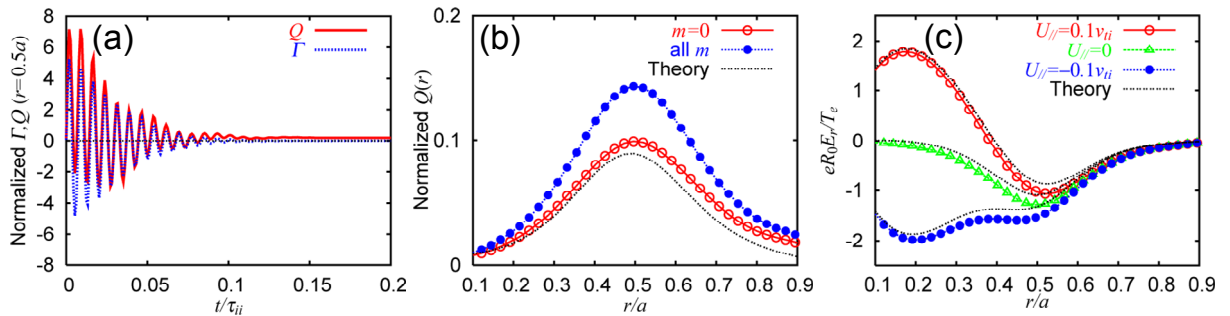


Fig.4: Neoclassical simulations using GT5D ( $(N_R, N_G, N_Z, N_{vi}, N_{v\perp}) = (160, 1, 160, 80, 20)$ ). (a) shows the particle flux  $\Gamma$  and the heat flux  $Q$  during GAM oscillations. (b) Steady  $Q$  is compared with Chang-Hinton's formula [10]. (c) Comparisons of steady  $E_r$  and Eq.(3) in simulations with Co, Zero, and Ctr toroidal rotation.

#### 4. Source driven ITG turbulence simulation

We simulate the same configuration as the ITG benchmark including  $C$  and  $S$ , and investigate long time behaviours of turbulent transport and profile formations over a collision time  $\tau_{ii}$ . Initial plasma profiles and source/sink deposition profiles are shown in Fig.5(a), and parameters at  $r_s \sim 0.5a$  are  $n_{0e} \sim 5 \times 10^{19} \text{m}^{-3}$ ,  $T_e \sim T_r \sim 2 \text{keV}$ ,  $R_0/L_n = 2.22$ ,  $R_0/L_{te} = 6.92$ ,  $R_0/L_{ti} = 10$ , and  $\nu^* \sim 0.02$ . A power scan with  $P_{in} = 2 \text{MW}$ ,  $4 \text{MW}$  is performed with  $\tau_s^{-1} = 0.1 v_{ti}/a$ . The time histories of the field and kinetic energy,  $\delta E_{fld}$ ,  $\delta E_{kin}$  and the power input/output due to the source/sink,  $E_{src}$ ,  $E_{snk}$  are shown in Fig.5(b). The simulation is initialized with  $f_{LM}$  as in the neoclassical benchmark, leading to the initial excitation of  $E_r$  and GAMs. After the damping

of GAMs, a kinetic equilibrium with  $E_r$  is formed. In this kinetic equilibrium, ITG modes glow and strong initial transient bursts are produced in the saturation processes of linear eigenmodes. This leads to quick adjustments of the  $T_i$  profile towards a nonlinear marginal state as in the ITG benchmark (Fig.4(a)). However, in source driven simulations, the  $T_i$  gradient is sustained above the critical value, where a power balance condition  $dE_{snk}/dt \sim dE_{src}/dt$  is established by the turbulent transport. In fig.5(b), the simulation keeps the energy conservation after subtracting  $E_{src} + E_{snk}$  from  $\delta E_{fld} + \delta E_{kin}$ , which shows a stringent verification of the simulation.

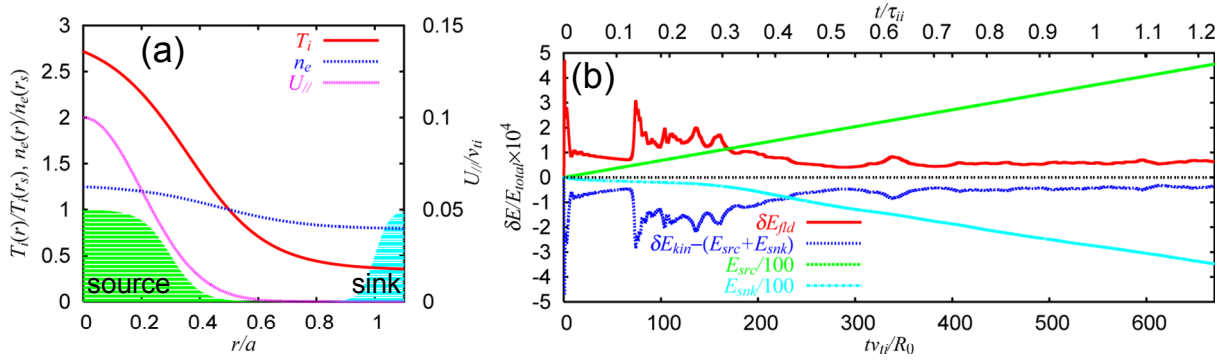


Fig.5: (a) Initial  $n_{0e}$ ,  $U_{\parallel}$ ,  $T_i$  profiles and source/sink deposition profiles. (b) Evolutions of the field and kinetic energy,  $\delta E_{fld}$ ,  $\delta E_{kin}$ , and input/output power from source/sink,  $E_{src}$ ,  $E_{snk}$ , in source driven ITG turbulence simulations using GT5D ( $P_{in}=2MW$ , 1/3wedge torus with  $n=0,3,\dots,48$ ,  $(N_R, N_{\zeta}, N_Z, N_{v\parallel}, N_{v\perp}) = (160, 32, 160, 80, 20)$ ).

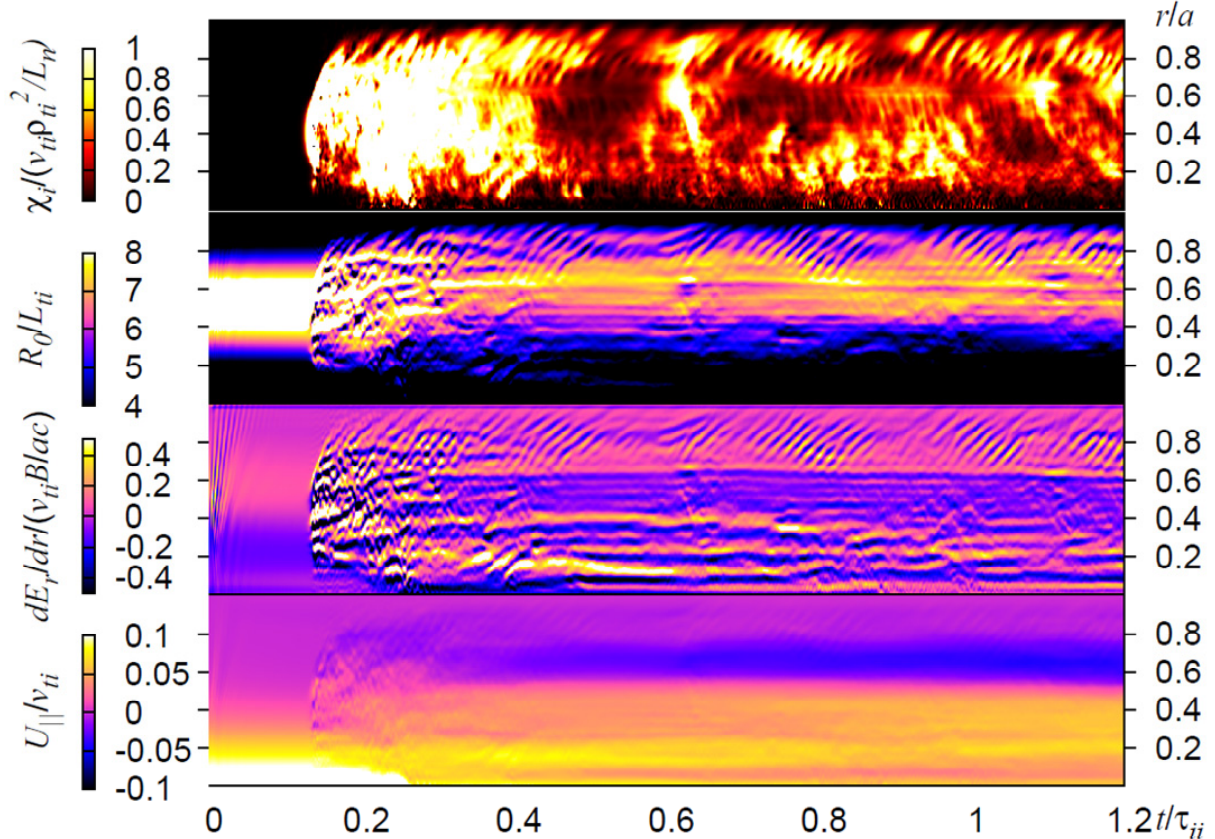


Fig.6: Spatio-temporal evolutions of (a) the ion heat diffusivity  $\chi_i$ , (b) normalized  $T_i$  gradient  $R_0/L_{Ti}$ , (c) the radial electric field shear  $dE_r/dr$ , and (d) the parallel flow velocity  $U_{\parallel}$  observed in the case with  $P_{in}=2MW$ .

**Power scan of heat transport and  $T_i$  profile** Although the time history of  $\delta E_{fld}$  suggests a quasi-steady turbulent state, Fig.6 indicates turbulent activities qualitatively different from previous gyrokinetic simulations with fixed gradients. Remarkable feature of source driven

ITG turbulence simulation is that the turbulent transport in a source free region ( $r/a=0.5\sim 0.9$ ) is dominated by avalanches (Fig.6(a)), and this region is tied to globally constant  $L_{ti}$  ( $R_0/L_{ti}\sim 7$ ), which is slightly above the nonlinear critical value ( $R_0/L_{ti}\sim 6$ ) (Figs.6(b) and 7(a)). While the radial correlation length  $\Delta r_c\sim 5\rho_{ti}$  and the correlation time  $\tau_c\sim 0.7R_0/v_{ti}\sim 2a/v_{ti}$  of the turbulent fields suggest a gyro-Bohm like picture, the propagation width and the fastest time scale of avalanches show an order of magnitude larger scales  $L_A\sim 20\rho_{ti}$  and  $\tau_A\sim 9R_0/v_{ti}$ . Their ballistic propagation velocity estimated from space-time autocorrelation analyses is  $V_A\sim \rho_{ti}v_{ti}/R_0$ . It is noted that in this simulation, GAM activities are not observed except for the initial phase, and the time scale of avalanches  $\omega_A\sim 2\pi/\tau_A\sim 0.7v_{ti}/R_0$  is significantly slower than GAMs  $\omega_{GAM}\sim 2v_{ti}/R_0$ . In the power scan, it is found that with increasing  $P_{in}$  from 2MW to 4MW,  $\chi_i$  is doubled with almost the same  $\Delta r_c$  and  $\tau_c$  and there is no significant change in  $R_0/L_{ti}$ , showing strong profile stiffness (Fig.7(a)). In Fig.7(b), it is shown that a significant part (50% $>$ ) of the turbulent heat flux  $Q$  is carried by avalanches, and their amplitudes significantly increase with  $P_{in}$ . These avalanches propagate with almost the same velocity, but the propagation width becomes shorter  $L_A\sim 10\rho_{ti}$  because of stronger  $T_i$  corrugation and local  $E_r$  shear, which suppress the ballistic propagation of avalanches. Although  $\tau_A$  is not changed so much, a quasi-periodic feature becomes weak in the autocorrelation function of  $Q$ , and an intermittent feature becomes strong. In Fig.7(c), the power spectrum of  $Q$  shows a small peak at  $\omega_A$ , where the power law changes from  $1/\omega$  to stronger decay. This kind of  $1/f$  type spectra, which was observed also in flux-driven fluid simulations [12] and in the experiment [13], are typically observed in a self-organised critical (SOC) system [14].

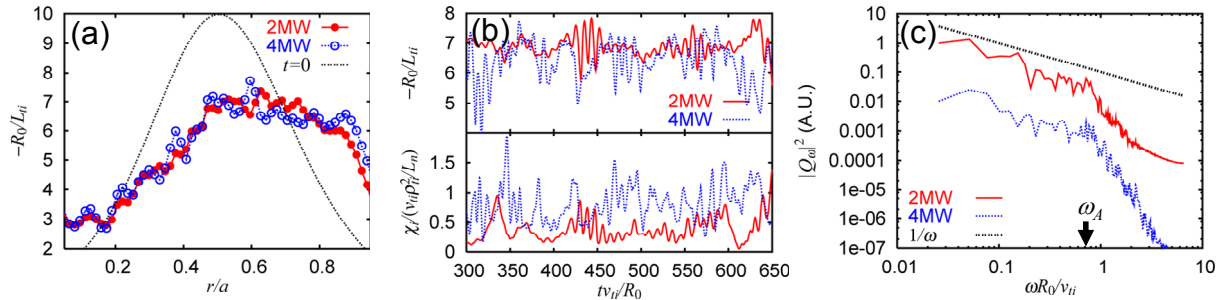


Fig.7: (a) Initial and steady (averaged over  $tv_{ti}/R_0=400\sim 650$ )  $L_{ti}$  profiles in the power scan with  $P_{in}=2MW, 4MW$ . (b) Time histories of  $L_{ti}$  and  $\chi_i$  observed at  $r/a=0.7$ . The time average of  $\chi_i/(v_{ti}\rho_{ti}^2/L_{ti})$  ( $tv_{ti}/R_0=400\sim 650$ ) is  $\sim 0.4$  and  $\sim 0.8$  for  $P_{in}=2MW$  and  $4MW$ , respectively and the neoclassical heat fluxes is less than  $\sim 0.1$  in the same unit. (c) Power spectrum of the turbulent heat flux  $Q$  averaged in a source free region at  $r/a=0.5\sim 0.9$ .

**Effects of  $E_r$  shear on avalanches and momentum transport** In Fig.6, not only  $\chi_i$  but also  $L_{ti}$  and  $dE_r/dr$  are showing similar avalanches. According to cross correlation analyses, both  $L_{ti}$  and  $E_r$  show a delay  $\Delta t\sim 1.5R_0/v_{ti}$  from  $\chi_i$ , but there is no delay between  $L_{ti}$  and  $E_r$ . This suggests that avalanching  $E_r$  is determined by some local equilibrium. It is noted that equilibrium  $E_r$  in source driven ITG turbulence simulations is significantly different from quasi-steady  $E_r$  in the collisionless ITG benchmark. In Fig.8(a), it is found that at  $r/a<0.5$ , quasi-steady  $E_r$  is close to the neoclassical level given by Eq.(3), and a small deviation due to zonal flows are observed. On the other hand,  $E_r$  at  $r/a>0.5$  is close to Eq.(3) with  $k=0$ , which is significantly larger than the neoclassical level, and avalanching components show a clear correlation with  $R_0/L_{ti}$ . The neoclassical benchmark shows that  $E_r$  approaches to the neoclassical level in collisional time scales in quiescent plasmas. However, in the avalanching region, the temperature gradient, which dictates the neoclassical poloidal flow, changes significantly in a faster time scale  $\tau_A\ll\tau_{ii}$  (Fig.7(b)). This may prevent a plasma from forming the neoclassical solution and provide  $E_r$  given by Eq.(3) with  $k\sim 0$ . The shear of equilibrium  $E_r$  affects propagation of avalanches. In Fig.6, the propagation direction of avalanches changes

depending on the sign of  $dE_r/dr$ . This can be understood also from  $E_r$  determined by  $R_0/L_{ti}$ . In the avalanche front, flattening of  $T_i$  occurs, and local maxima of  $E_r$  and  $R_0/L_{ti}$  are produced (Fig.8(a)). As a result, the avalanche front is bounded by positive and negative local  $E_r$  shear regions (Fig.8(b)). In the positive (negative) mean  $E_r$  shear region, local  $E_r$  shear in the outside (inside) is always weak, and ITG modes in the avalanche front tend to couple with modes in the outside (inside), leading to one-sided propagation of avalanches. Another important effect of the  $E_r$  shear is its influence on the momentum transport. In the present work, initial flows with  $U_{||} \sim 0.1v_{ti}$  are given in the co-current direction, and the momentum diffusion is observed during initial transient bursts. However, in Fig.6(d), it is found that steady parallel flows are sustained without momentum input near the axis, suggesting an existence of a non-diffusive momentum flux. In Fig.8(c), a correlation between the momentum flux  $\Pi$  and  $dE_r/dr$  is clearly seen, and  $\Pi$  is outward (inward) in a positive (negative)  $dE_r/dr$  region at  $r/a > 0.6$  ( $r/a = 0.4 \sim 0.6$ ). As a result,  $U_{||}$  in the co-current direction is sustained at  $r/a < 0.5$ , while  $U_{||}$  in the counter-current direction is peaked at  $r/a \sim 0.6$ . It is noted that  $U_{||}$  and  $E_r$  are determined self-consistently through Eq.(3) and the momentum flux affected by  $dE_r/dr$ . Since the initial toroidal rotation is almost zero at  $r/a = 0.4 \sim 1$ , the non-diffusive momentum flux is qualitatively consistent with a  $E \times B$  shear stress reported in [15].

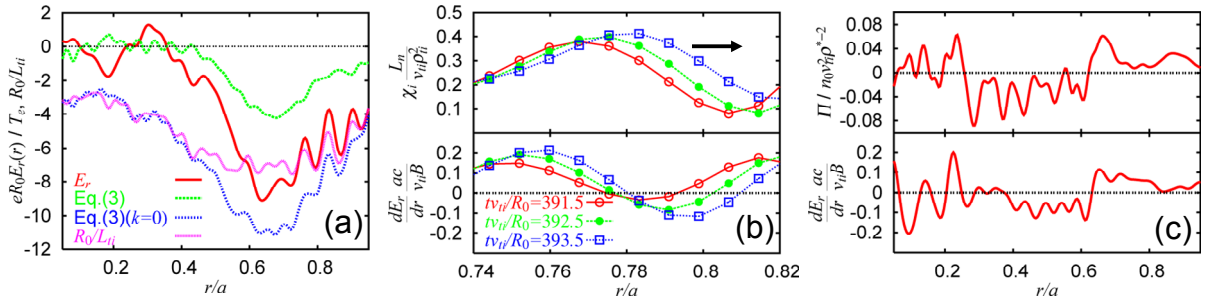


Fig. 8: (a)  $E_r$  profile at  $tv_{ti}/R_0 \sim 550$ . Also shown are  $L_{ti}$  and  $E_r$  calculated from Eq.(3) and Eq.(3) with  $k=0$ . (b) radial propagation of avalanche fronts, which is bounded by positive and negative  $E_r$  shear shifted by mean  $E_r$ . (c) Radial profiles of the momentum flux  $\Pi$  and  $dE_r/dr$  averaged over  $tv_{ti}/R_0 = 400 \sim 650$ .

## 5. Summary

A new global gyrokinetic toroidal full- $f$  5D Vlasov simulation GT5D is developed based on the modern gyrokinetic theory and the linear FP collision operator. Important features of GT5D are 1) robust and accurate long time full- $f$  simulations enabled by the NDCFD, 2) neoclassical physics represented by the linear FP collision operator, 3) flexible choices (extensions) of experimentally relevant source models, and 4) full radius treatment of shaped MHD equilibria. The code is carefully verified through the linear and nonlinear benchmarks against GT3D and the neoclassical benchmarks. In the collisionless ITG benchmark, two gyrokinetic codes with completely different numerical approaches identify the same global solution of ITG turbulence. In the neoclassical benchmark, standard local theories are recovered by axisymmetric simulations using GT5D. However, it is found that 1) significant heat flux is driven by GAM oscillations, 2) additional heat flux is produced with  $m \neq 0$ ,  $n = 0$  component of  $\phi$ , and 3)  $E_r$  approaches to the neoclassical level slowly in collisional time scales starting from initial  $E_r$  which is significantly larger than the neoclassical level. Source driven ITG simulations in a normal shear tokamak with  $\rho^{*-1} \sim 150$  and  $\nu^* = 0.02 \sim 0.1$  are performed using source/sink models to fix power input (zero momentum input) near the axis and  $T_i$  ( $U_{||} \sim 0$ ) at the edge. In the simulation, long time behaviours of the turbulent transport and profile formations are simulated over a collision time, several key features in the experiment are recovered. We found that 1) stiff  $T_i$  profiles with globally constant  $L_{ti}$ , which

are typically observed in H-mode plasmas [16], are sustained in source free regions, 2) in these regions, a significant part of the heat flux is carried by avalanches which have an order of magnitude larger spatio-temporal scales than the turbulent correlation length  $\Delta r_c$  and time  $\tau_c$ , 3) in the power scan, amplitudes of avalanches are enhanced with almost the same  $\Delta r_c$  and  $\tau_c$ , and the intermittent heat flux shows  $1/f$  type spectra, which was observed also in the experiment [13], 4) the equilibrium  $E_r$  in avalanching regions is significantly larger than the neoclassical level, and its shear dictates the direction of the avalanche propagation and the momentum flux, and 5) without momentum input near the axis, a momentum pinch keeps non-zero toroidal rotation (parallel flows) in the co- (counter-) current direction in the core (outer) region, which may be related to the intrinsic toroidal rotation [17]. These features are qualitatively different from previous fixed gradient  $\mathcal{J}$  simulations, and may be crucial for direct comparisons with the experiment, which will be addressed in future works.

We would like to thank Drs. M. Ida, N. Hayashi, M. Honda, M. Yoshida, Y. Kamada, M. Kikuchi, S. Satake, T. H. Watanabe, H. Sugama, and P. H. Diamond for useful discussions. The simulations were performed on the JAERI Altix3700Bx2 system. One of the author (Y. I.) is supported by the MEXT, Grant No. 18760647.

## References

- [1] IDOMURA, Y., et al., "Conservative global gyrokinetic toroidal full- $f$  five dimensional Vlasov simulation", *Comput. Phys. Commun.* 179 (2008) 391.
- [2] IDOMURA, Y., et al., "New conservative gyrokinetic full- $f$  Vlasov code and its comparison to gyrokinetic  $\mathcal{J}$  particle-in-cell code", *J. Comput. Phys.* 226 (2007) 244.
- [3] IDOMURA, Y., et al., "Global gyrokinetic simulation of ion temperature gradient driven turbulence in plasmas with canonical Maxwellian distribution", *Nucl. Fusion* 43 (2003) 234.
- [4] BRIZARD, A. J., et al., "Foundations of nonlinear gyrokinetic theory", *Rev. Mod. Phys.* 79 (2007) 421.
- [5] ZHONG, X., "Additive semi-implicit Runge-Kutta methods for computing high speed nonequilibrium reactive flows", *J. Comput. Phys.* 128 (1996) 19.
- [6] XU, X. Q., et al., "Numerical simulation of ion-temperature-gradient-driven modes", *Phys. Fluids B* 3 (1991) 627.
- [7] WANG, W. X., et al., "A new  $\mathcal{J}$  method for neoclassical transport studies", *Plasma Phys. Control. Fusion* 41 (1999) 1091.
- [8] SUGAMA, H., et al., "Collisionless damping of zonal flows in helical systems", *Phys. Plasmas* 13 (2006) 012501.
- [9] DIMITS, A. M., et al., "Comparisons and physics basis of tokamak transport models and turbulence simulations", *Phys. Plasmas* 7 (2000) 969.
- [10] CHANG, C. S., et al., "Effect of finite aspect ratio on the neoclassical ion thermal conductivity in the banana regime", *Phys. Fluids* 25 (1982) 1493.
- [11] HINTON, F. L., et al., "Theory of plasma transport in toroidal confinement systems", *Rev. Mod. Phys.* 48 (1976) 239.
- [12] GARBET, X., et al., "Heat flux driven ion turbulence", *Phys. Plasmas* 5 (1998) 2836.
- [13] POLITZER, P. A., "Observation of avalanche like phenomena in a magnetically confined plasma", *Phys. Rev. Lett.* 84 (2000) 1192.
- [14] BAK, P., et al., "Self-organized criticality: an explanation of  $1/f$  noise", *Phys. Rev. Lett.* 59 (1987) 381.
- [15] GURUCAN, O. D., et al., "Intrinsic rotation and electric field shear", *Phys. Plasmas* 14 (2007) 042306.
- [16] URANO, H., et al., "Dependence of heat transport on toroidal rotation in conventional H-modes in JT-60U", *Nucl. Fusion* 48 (2008) 085007.
- [17] YOSHIDA, M., et al., "Role of pressure gradient on intrinsic toroidal rotation in tokamak plasmas", *Phys. Rev. Lett.* 100 (2008) 105002.